

Inhomogeneous microstructure and mechanical properties of friction stir processed NiAl bronze

D.R. Ni, P. Xue, D. Wang, B.L. Xiao, Z.Y. Ma*

Shenyang National Laboratory for Materials Science, Institute of Metal Research, Chinese Academy of Sciences, 72 Wenhua Road, Shenyang 110016, China

ARTICLE INFO

Article history:

Received 27 March 2009

Accepted 5 June 2009

Keywords:

Friction stir processing
Bronze
Microstructure
Mechanical properties

ABSTRACT

As-cast Cu–9Al–4.5Ni–4Fe NiAl bronze (NAB) alloy was subjected to friction stir processing (FSP) in a wide range of tool rotation rates of 800–2000 rpm and traverse speeds of 50–200 mm/min. After FSP, the initial coarse microstructure of the as-cast NAB was transformed to fine structure, and the porosity defects were eliminated. However, the stir zones were characterized by inhomogeneous structure and could be divided into four regions: fine Widmanstätten primary α phase in the surface layer, banded primary α and β' phases in the subsurface layer, equiaxed α and β' phases in the center, and streamlike α and β' phases at the bottom. The heterogeneous microstructure could be alleviated by adjusting the FSP parameters, but could not be completely eliminated under investigated FSP parameters. The FSP NAB exhibited significantly improved hardness, tensile strength, and ductility compared to the base metal. When the NAB was subjected to two pass FSP, its microstructure was further homogenized, resulting in apparently increased ductility with similar hardness and tensile strength.

© 2009 Elsevier B.V. All rights reserved.

1. Introduction

Based on the basic principles of friction stir welding (FSW), invented at The Welding Institute (TWI), UK at 1991 [1–4], friction stir processing (FSP) has been developed as a rising metal working method. This processing technique was firstly used by Mishra et al. to produce fine-grained aluminum alloys [5,6]. Subsequently, this multifunctional technique was employed to modify the microstructure of heterogeneous metallic materials [7], to produce surface composites [8,9], and to synthesize composites and intermetallic compounds [10,11]. One of the most promising applications of FSP is to provide localized modification and control of microstructures in near surface layers of the as-cast components without changing their shape, with the porosities being eliminated and the inclusions being redistributed [12]. After FSP, the initial as-cast microstructure was converted into wrought structure, and the microstructure refinement, homogenization, and densification resulting from FSP enhanced the mechanical properties of the castings effectively.

NiAl bronze (NAB) alloys are widely used for marine components due to their good combination of strength, fracture toughness, and corrosion resistance [13–17]. As a quaternary alloy, the transformation products and their precipitation sequence in the NAB alloys are complex during slow cooling. The as-cast NAB is mainly composed of coarse Widmanstätten α phase, nickel–iron–aluminum κ

phases, and island martensite β' phase, and there are some shrinkage porosity defects in the castings [18–23]. In order to improve the mechanical properties of the cast NAB, it is necessary to modify the microstructure of the castings. However, it seems that no suitable techniques were established to modify the structure of NAB castings until the appearance of the FSP.

Recently, investigations on the FSP of the cast NAB alloys have been conducted with the aim to repair defects and to refine and homogenize the coarse microstructures, strengthening the surface of as-cast components locally. It was reported that the U.S. Naval Surface Warfare Center, Carderock Division (NSWCCD) investigated the potential of FSP as a repair tool for eliminating surface defects and locally strengthening the surface of NAB ship propellers, with the aim to increase its service life and performance [24]. It has been shown that FSP increased the hardness, tensile properties, and fatigue strength of the as-cast NAB without affecting the corrosion behavior in neutral salt solution [24–27].

In the past few years, a number of studies were conducted to understand the microstructure evolution of the cast NAB during FSP. Oh-ishi et al. [28–32] studied the microstructures of the FSP NAB, Cu–9Al–5Ni–4Fe–1Mn (UNS C95800), in detail. It was shown that the main characteristic of the stir zone (SZ) of the FSP NAB was inhomogeneous microstructures, including Widmanstätten structure, equiaxed fine grain structure, and banded or lamellar structure, and the processing parameters affected the microstructures and temperature distribution in the FSP NAB apparently. Mahoney et al. [25] and Fuller et al. [33] also studied the microstructure of FSP NAB. The microstructures they reported were similar to those

* Corresponding author. Tel.: +86 24 83978908; fax: +86 24 83978908.
E-mail address: zyna@imr.ac.cn (Z.Y. Ma).

Table 1
Composition of NAB UNS C95800 (wt.%).

Al	9.18
Ni	4.49
Fe	4.06
Mn	1.03
Cu	Balance

Table 2
FSP parameters and sample designations.

Rotation rate (rpm)	Traversing speed (v , mm/min)		
	50	100	200
800	FSP-800/50	–	–
1000	FSP-1000/50	–	–
1200	FSP-1200/50	FSP-1200/100	–
1500	FSP-1500/50	FSP-1500/100	FSP-1500/200
2000	–	FSP-2000/100	–
1200	FSP-1200/50 × 2 ^a	–	–

^a Two pass FSP.

reported by Oh-ishi et al. [28–32]. However, those inhomogeneous microstructures, especially the banded structures, were still not well understood.

On the other hand, although the microstructure evolution of the NAB during FSP has been reported in several studies, the range of the FSP parameters (rotation rate and traversing speed) is relatively narrow. Furthermore, the information on the effect of FSP on the mechanical properties is limited. In this study, FSP on cast Cu–9Al–4.5Ni–4Fe was conducted under a wide range of FSP parameters, the microstructure and mechanical properties were examined. The aim is to establish the correlation between FSP parameters, microstructure and mechanical properties of the cast NAB.

2. Experimental

10 mm thick commercial UNS C95800 NAB alloy cast plates were used in this study, and the composition of the NAB is shown in Table 1. The as-received NAB plates were machined into pieces of 300 mm × 70 mm × 8 mm and subjected to FSP under a wide range of tool rotation rates and traverse speeds as shown in Table 2. The FSP samples were nominated as FSP—a series digital format. For example, sample FSP-800/50 denotes that the sample was FSPed at a rotation rate of 800 rpm and a traversing speed of 50 mm/min. A tool tilt angle of 3° was used for all FSP operations. A nickel-based alloy tool with a concave shoulder 24 mm in diameter, and a threaded conical pin 8 mm in root diameter and 6 mm in length was used. Both the tool and the processed piece were subjected to blow over cooling during FSP. In order to investigate effect of multiple-

pass on microstructure and mechanical properties of NAB, a two pass FSP with a 100% overlap and the same forward directions was conducted on the NAB.

The microstructure and element distribution of the base metal (BM) and the FSP samples were examined using optical microscopy (OM) and electron probe micro-analyzer (EPMA). The hardness profiles were measured on the transverse cross-section of the SZ along horizontal and vertical directions, respectively, by using a micro-vickers hardness tester with a load of 5 kg for 15 s. Transverse and longitudinal mini-tensile specimens containing only the SZ, with a gage length of 5 mm, a gage width of 1.5 mm, and a gage thickness of 0.85 mm, were machined from the center of the SZ of the FSP samples perpendicular and parallel to the FSP direction, respectively. For the purpose of comparison, tensile specimens with a large gage dimension of 60 mm × 12 mm × 8 mm were machined from the as-cast NAB. Tensile tests were conducted at a strain rate of $1 \times 10^{-3} \text{ s}^{-1}$ at room temperature, using an Instron 5848 tensile tester for the FSP specimens and an AG-100KNG tensile tester for the as-cast specimens, respectively. The property data for each condition were obtained by averaging four test results.

3. Results

3.1. Optical microstructure

The as-cast structure of the NAB was characterized by coarse Widmanstätten α phase, coarse martensite β' phase, fine κ phase particles, as well as some casting porosities (Fig. 1). The light-etching phase with a size of $\sim 150 \mu\text{m}$ was the α phase, whereas the dark-etching constituents were associated with the various β transformation products. Fig. 2 shows macrographs of the SZs. FSP parameters had a slight effect on the macrostructure of the SZs. Under the investigated FSP parameters, all the SZs showed the similar basin-like shape with a wide top region. The traversing speed affected the area of the SZs more evidently compared to the rotation rate. At a constant rotation rate of 1200 or 1500 rpm, with an increase in the traverse speed from 50 to 100 mm/min or from 50 to 200 mm/min, the area of the SZs decreased, and the FSP-1500/200 sample possessed the smallest area among all the SZs. When the two pass FSP was conducted, the area of the SZ increased apparently. FSP refined the coarse as-cast microstructure and eliminated the casting defects of shrinkage porosity and void in the BM, producing densified fine-grained structure (Fig. 3). Three distinct zones, SZ, thermomechanically affected zone (TMAZ), and heat-affected zone (HAZ) could be identified based on the microstructural characterizations (Figs. 2 and 3). The interface between the SZ and the TMAZ was sharp on the advancing side (AS), whereas it was diffuse on the retreating side (RS) and under the tool. A macroscopically visible banded structure and “onion ring” pattern were observed in the

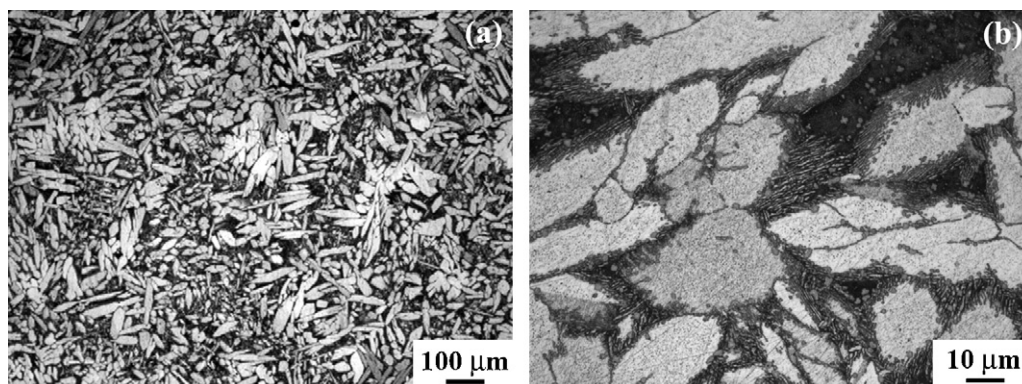


Fig. 1. Optical micrographs of as-cast NAB showing: (a) Widmanstätten morphology and porosities at low magnification and (b) precipitates at high magnification.

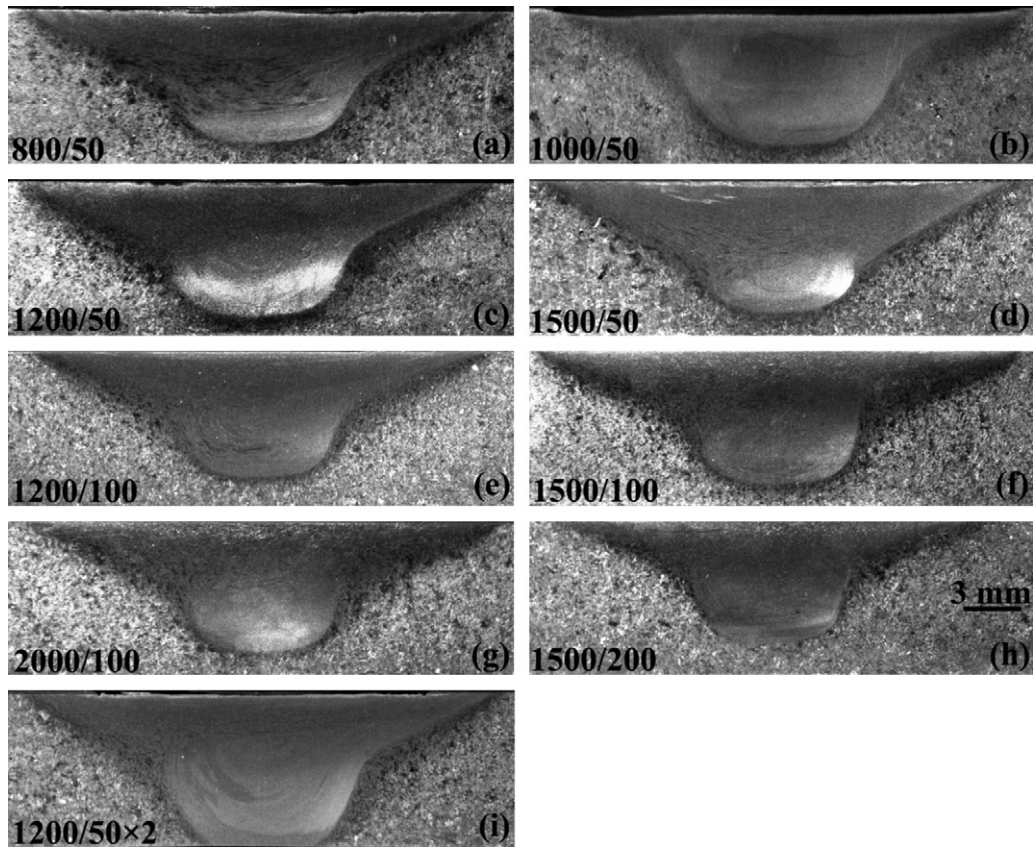


Fig. 2. Optical cross-sectional macrograph of FSP samples prepared at various parameters.

upper part and around the center of the SZ, respectively, indicating that the inhomogeneous microstructures appeared in the SZ.

Based on the microstructures, the SZs for all FSP parameters could be divided into four sub-regions from the surface to the bottom as indicated in Fig. 3. Region A below the surface was associated with distinct Widmanstätten primary α phase (Fig. 4a). Region B in the subsurface consisted of elongated banded primary α and β' phases (Fig. 4b). This microstructural feature is more apparent in the RS of the SZ than in the AS. Region C in the center of the SZ was composed of equiaxed α and β' phases (Fig. 4c), with the size of the α phase being less than $10\ \mu\text{m}$. In region D at the bottom of the SZ, the streamlike α phase with a grain size of $2\text{--}3\ \mu\text{m}$ intermingled with dark-etching β transformation products (Fig. 4d). Both the banded structure in region B and the streamlike structure in region D were elongated and generally aligned in the horizontal direction. Meanwhile, annealing twins were detected in the α phase, especially in the banded and streamlike α structure.

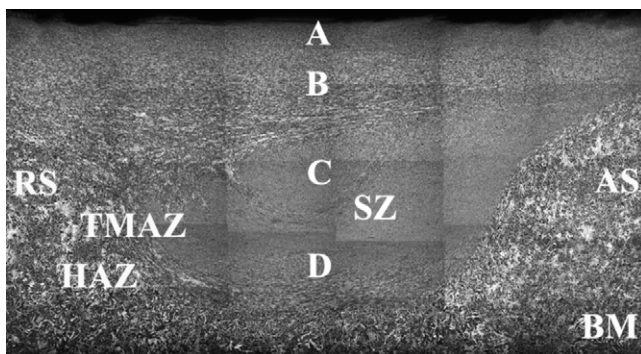


Fig. 3. Montage of optical micrographs from cross-sections of FSP-1200/50 sample.

It should be noted that the inhomogeneous microstructure of the onion ring pattern was apparently parameter dependent (Fig. 5). Generally, compared to those at a lower traversing speed of $50\ \text{mm}/\text{min}$ (Fig. 5a–d), the onion ring patterns in the SZs at higher traversing speeds of 100 and $200\ \text{mm}/\text{min}$ were more apparent (Fig. 5e–h). At the traversing speed of $50\ \text{mm}/\text{min}$, the SZ of the FSP-800/50 sample showed the most apparent onion ring pattern (Fig. 5a), whereas the SZ of the FSP-1000/50 sample exhibited the most homogeneous microstructure with the largest area of equiaxed structure among all the SZs (Fig. 5b). With the rotation rate further increased to 1200 and $1500\ \text{rpm}$, the onion ring pattern became more apparent.

The onion rings appeared below the banded structure region. At lower rotation rates of 800 and $1000\ \text{rpm}$, ringlike bands were composed of layers of elongated α grains and equiaxed α grains, surrounded by fine β phase transformation products (Fig. 6a). At higher rotation rates of 1200 , 1500 and $2000\ \text{rpm}$, the onion rings consisted of layers of Widmanstätten α and layers of mixed equiaxed α and β transformation products (Fig. 6b).

For the two pass FSP, four sub-regions as mentioned above still existed in the SZ. However, after the two pass FSP, the inhomogeneous structure was greatly improved and the area of equiaxed structure in the SZ increased apparently, and the onion ring pattern was almost eliminated (Fig. 7). However, the elongated banded structure still existed in the SZ of the two pass FSP sample, which was similar to that of the one pass FSP sample.

3.2. EPMA microstructure

EPMA examinations showed that the as-cast NAB was composed of coarse Widmanstätten α phase (white color), κ phase particles (dark color), and small areas of retained “island” martensite

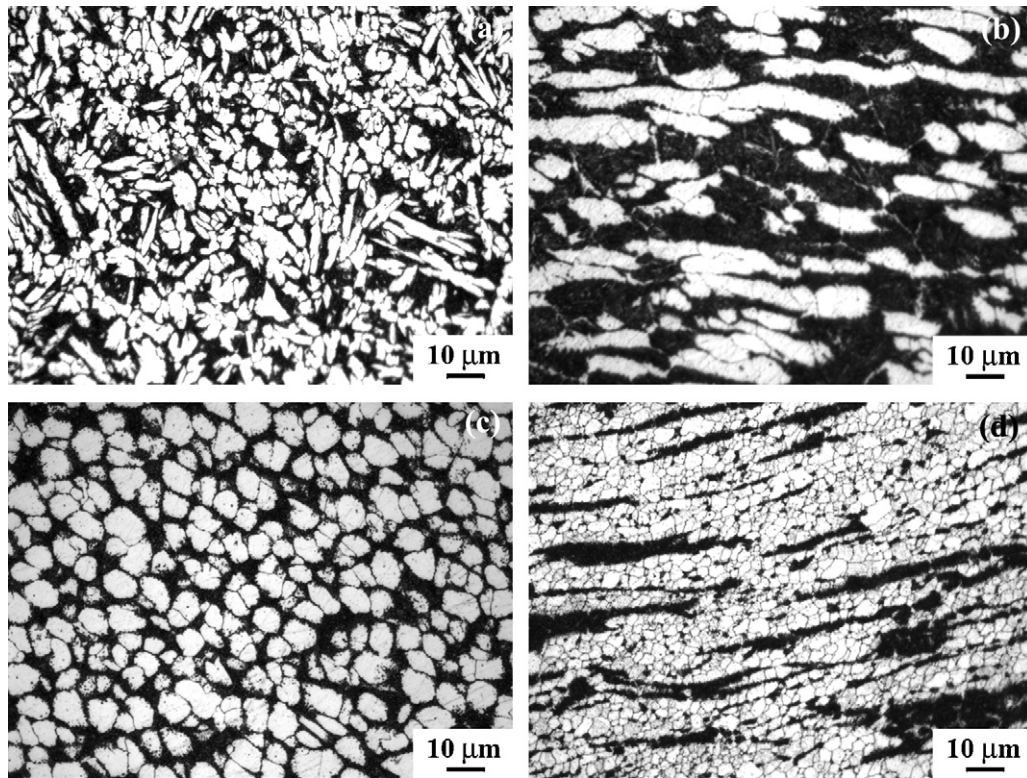


Fig. 4. Optical micrographs of stir zone (FSP-1250/50) showing different microstructures at: (a) location A, (b) location B, (c) location C and (d) location D in Fig. 3.

β' phase (grey color), and most of the κ phases were inhomogeneously distributed on the interface between the α and β' phases (Fig. 8a). After FSP, the coarse Widmanstätten α and β transformation products were greatly refined, and the κ phases were uniformly distributed (Fig. 8b). The microstructures revealed by EPMA are in agreement with the OM microstructures. Furthermore, EPMA analyses revealed that FSP alleviated the severe composition segregation in the cast NAB. After FSP, the element Ni and Fe were uniformly distributed around equiaxed α particles (Fig. 8c–f).

3.3. Microhardness

The hardness profiles of the FSP-1200/50 sample are showed in Fig. 9. Three important observations can be made. First, the hardness value of the SZ was significantly higher than that of the BM (Fig. 9a). Second, the hardness value in the center of the SZ was slightly lower than that near the surface and the bottom (Fig. 9b). Third, both the one pass and two pass FSP samples showed a similar hardness distribution and hardness value. However, the two pass FSP sample exhibited more homogeneous hardness distribution in the SZ than the one pass FSP sample (Fig. 9a).

3.4. Tensile properties

The tensile properties of the FSP NAB samples prepared at various parameters are shown in Table 3. Five important findings can be revealed from Table 3. First, all the FSP samples exhibited significantly improved tensile strength and ductility compared to the BM. The yield strength (YS), ultimate tensile strength (UTS), and elongation of the FSP samples were 436–502 MPa, 790–852 MPa, and 20–29%, respectively, along the transverse direction, and 415–479 MPa, 776–837 MPa, and 25–31%, respectively, along the longitudinal direction. Second, the tensile properties were parameter dependent. For a constant traversing speed of 50 or 100 mm/min, with increasing the rotation rates from 800 to

1500 rpm or from 1200 to 2000 rpm, the YS and UTS of the FSP samples increased firstly and then decreased. For a constant rotation rate of 1200 rpm, increasing the traversing speed led to lower UTS; however, at 1500 rpm, increasing the traversing speed from 50 to 200 mm/min led to an increase in the UTS first and then a decrease. With the stir tool used, when the rotation rates of 1000–1500 rpm and the traversing speeds of 50–100 mm/min were used, good tensile properties could be achieved in the FSP NAB samples. Third, among the one pass FSP samples, the FSP-800/50 sample showed the lowest elongation, whereas the FSP-1000/50, FSP-1200/50, and FSP-1500/50 samples exhibited better ductility than the others. Fourth, the YSs of the FSP samples along the transverse direction were slightly higher than those along the longitudinal direction. Fifth, the two pass FSP improved the elongation of the samples apparently, which increased by 24% compared to the one pass FSP, however, the two pass FSP did not apparently affect the tensile strength.

4. Discussion

4.1. Microstructural characteristics

The addition of Ni and Fe into binary Cu–Al alloys extends the apparent range of the α field and generates κ phases to suppress the formation of γ phase (Al_4Cu_9) which is deleterious to the corrosion resistance of the NAB [13]. The phases and phase transformation sequence of NAB are complex (Fig. 10). The cast NAB is characterized by coarse microstructure, severe composition segregation, and shrinkage porosity defects, which reduce the mechanical properties and corrosion resistance of the NAB castings. FSP resulted in the significant breakup and decomposition of coarse Widmanstätten α phase and κ phases, the closure of casting porosities, and the uniform distribution of phases. After one pass FSP, the as-cast microstructure of the BM was greatly refined. However, the microstructure of the SZ was inhomogeneous. Similar results have

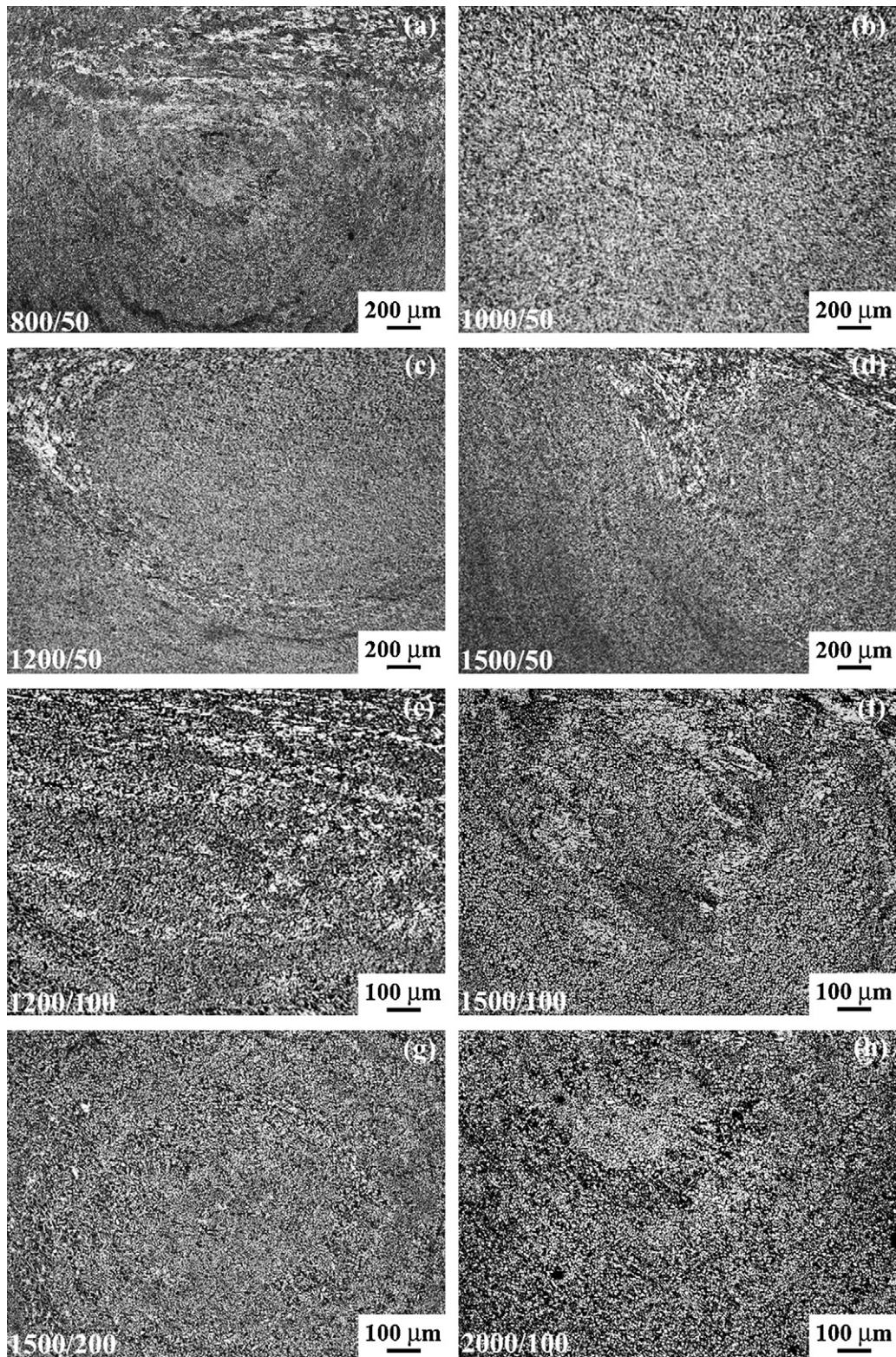


Fig. 5. Optical cross-sectional macrographs in center of onion ring of stir zones prepared at various parameters.

been previously reported in the FSP NAB samples by other investigators [28–31,33]. Considering the fact that the crystal structure and the evolution of the κ phases during FSP have been reported in detail elsewhere [28], in this study we mainly focus on the inhomogeneous microstructure in the SZ.

During FSP, various regions in the SZ experienced different thermomechanical histories. Oh-ishi et al. [30] estimated the local

peak temperatures in the SZ of FSP NAB according to the different microstructures and phases. They considered that during FSP the temperature distribution was different in various regions of the SZ, and the surface experienced the highest temperature, whereas the bottom underwent the lowest temperature. When the rotation rate was higher than 800 rpm, the surface temperature was estimated to be about 1030 °C, the 1/3 depth location was about 930 °C, and

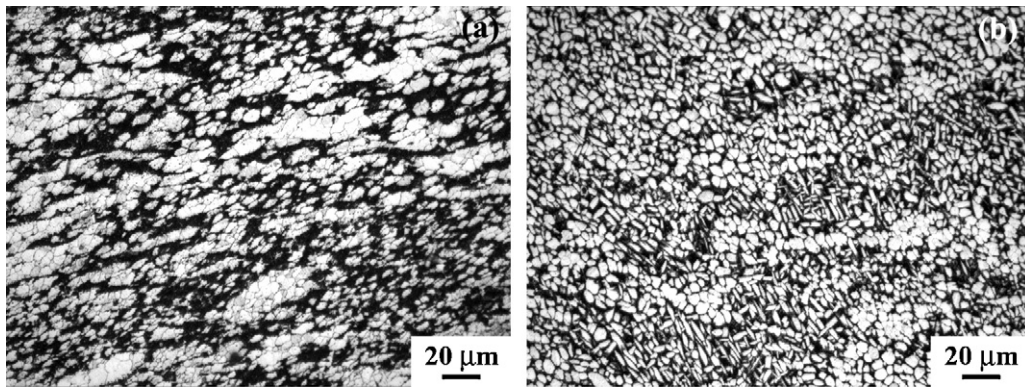


Fig. 6. Optical micrographs showing ringlike bands in stir zones in: (a) FSP-800/50 and (b) FSP-1500/200.

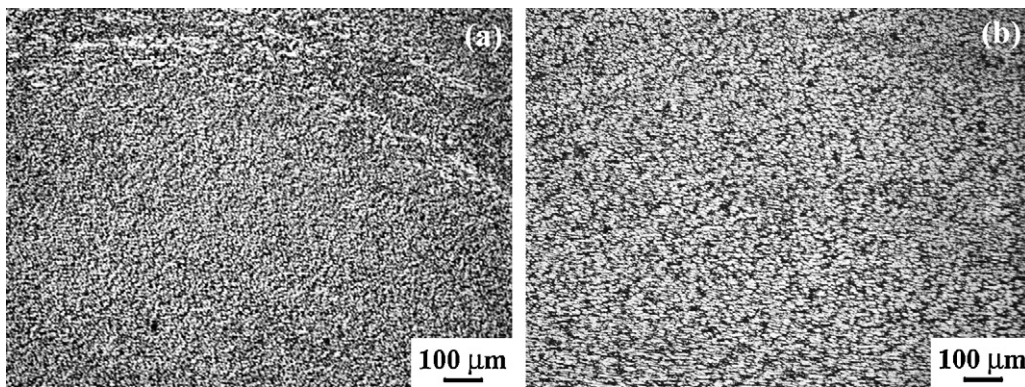


Fig. 7. Optical microstructure in center of stir zone (FSP-1200/50): (a) one pass and (b) two pass.

the bottom was higher than 800 °C [30]. The surface layer of the SZ experienced the highest temperature higher than 930 °C, and the material in this region was transformed into single β phase (Fig. 10).

During the following cooling process, the fast cooling rate resulted in that Widmanstätten α phase as well as bainite and martensite appeared in this region (Fig. 4a). In the region further

below the surface, the temperature was lower than that of the surface, but it is higher than the α/β transformation temperature. So, partial α phase transformed into the β phase and then decomposed during the following cooling process. There was apparently elongated banded α structure with large size in this region. It seems that the banded α structure came from the blocklike α phase in

Table 3
Tensile properties of FSP NAB prepared at various FSP parameters.

Sample	Direction	Tensile properties		
		YS (MPa)	UTS (MPa)	EL (%)
FSP-800/50	Transverse	465 ± 4.9	775 ± 32	20 ± 5.3
	Longitudinal	479 ± 37	822 ± 12	25 ± 5.9
FSP-1000/50	Transverse	494 ± 0.6	795 ± 1.5	29 ± 3.1
	Longitudinal	466 ± 22	837 ± 3.1	29 ± 4.0
FSP-1200/50	Transverse	502 ± 21	838 ± 12	29 ± 1.5
	Longitudinal	469 ± 17	804 ± 15	28 ± 6.9
FSP-1500/50	Transverse	480 ± 41	790 ± 29	28 ± 4.0
	Longitudinal	472 ± 37	776 ± 31	28 ± 7.9
FSP-1200/100	Transverse	467 ± 32	796 ± 26	25 ± 1.7
	Longitudinal	465 ± 17	793 ± 26	31 ± 4.2
FSP-1500/100	Transverse	495 ± 34	852 ± 11	28 ± 2.9
	Longitudinal	466 ± 24	815 ± 12	27 ± 1.7
FSP-2000/100	Transverse	436 ± 10	804 ± 8	25 ± 1.7
	Longitudinal	415 ± 16	805 ± 22	25 ± 1.7
FSP-1500/200	Transverse	473 ± 28	838 ± 15	24 ± 1.2
	Longitudinal	440 ± 24	826 ± 25	25 ± 3.8
FSP-1200/50 × 2	Transverse	498 ± 36	810 ± 5	37.9 ± 1.9
	Longitudinal	455 ± 19	814 ± 13	34.5 ± 2.8
Base metal	–	282 ± 2	645 ± 29	18 ± 6.6

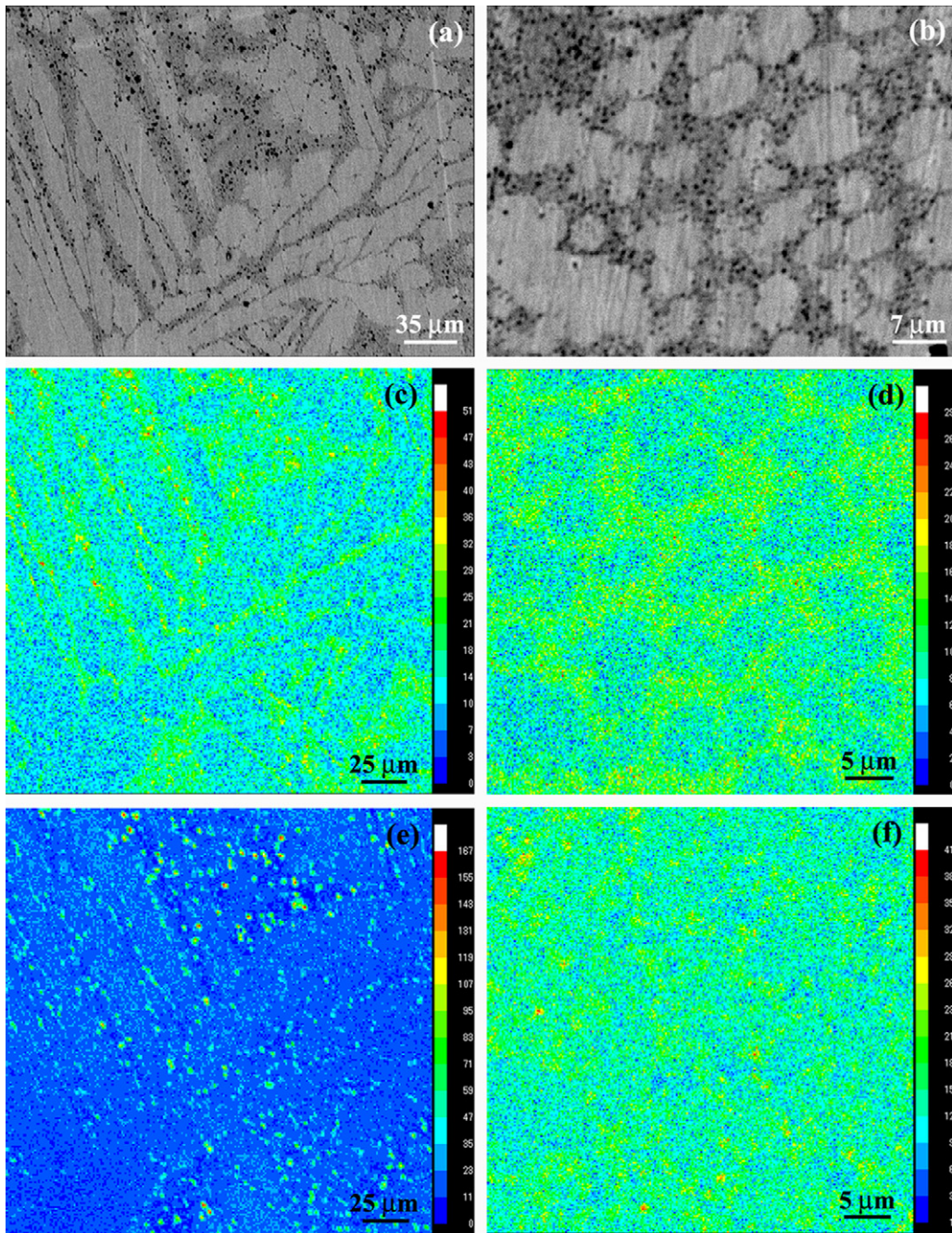


Fig. 8. EPMA results of as-cast (a, c, and e) and FSP-1200/50 (b, d, and f) showing microstructure and element distribution: (a and b) BSE images; (c and d) distribution of Ni; (e and f) distribution of Fe.

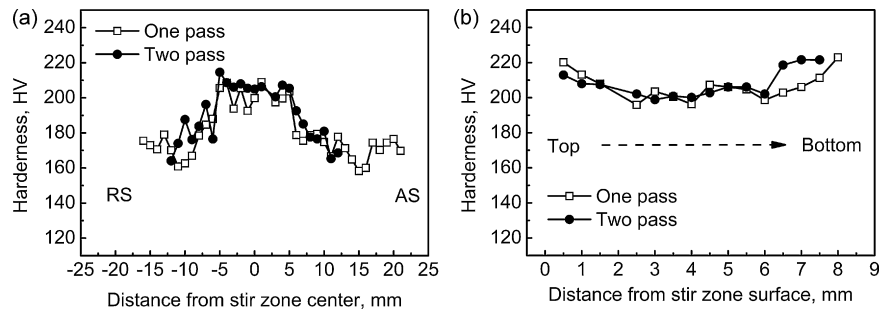


Fig. 9. Microhardness profiles of cross-section of stir zone (FSP-1200/50) along (a) horizontal and (b) vertical directions.

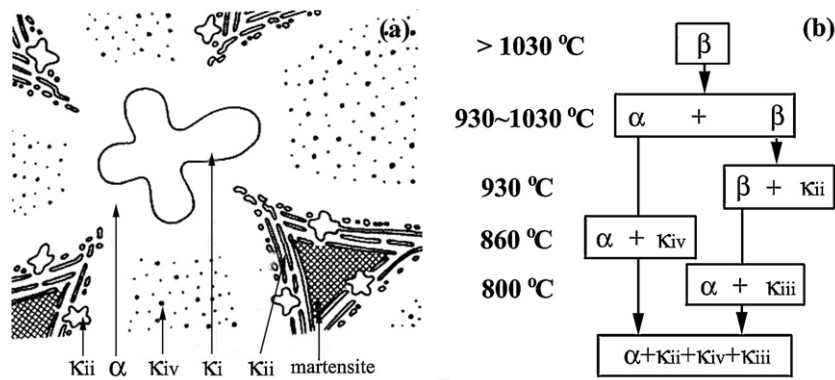


Fig. 10. Schematic diagram of: (a) as-cast microstructure of equilibrium cooled NAB and (b) sequence of transformations during cooling [23,28].

the BM due to the severe deformation. Most of the banded α structure was distributed on the upper part of the RS but little in the AS, and this confirms that the banded α structure would come from the RS by the material flow resulting from the rotation tool. During FSP, the BM structure underwent severe deformation, and the dynamic recrystallization appeared. However, most α structure retained despite the severe deformation. This explained the decrease of Widmanstätten α phase and the increase of elongated banded α in this region (Fig. 4b).

In the center of the SZ, few α phase and partial κ phase transformed into the β phase, and most of the α phase converted into equiaxed grains due to the dynamic recrystallization resulting from severe deformation. Consequently, the equiaxed α and β transformation products appeared in this region (Fig. 4c). In the bottom of the SZ, the temperature is the lowest and no α was transformed. The material in this region suffered from severe deformation resulting from the stirring and breaking effect of the rotation tool. The streamlike structures were formed and then equiaxed fine grains generated within the streamlike pattern due to the dynamic recrystallization. With the rapid cooling rate the growth of the newly formed fine grains was inhibited, therefore, the grain size in this region was the finest (Fig. 4d). Consequently, equiaxed fine α grains were achieved in the form of elongated streamlike patterns.

The cooling condition should be also responsible for the microstructure of the SZ. During the following cooling process, various locations in the SZ experienced different cooling rates from the surface to the bottom. The surface was subjected to the blowing air so its cooling rate was fast, and the bottom was close to the steel backing so its cooling rate was the fastest, whereas the cooling rate for the inner part of the SZ was relatively slow. As a result, the fast cooling rates are of benefit to the formation of fine microstructure.

The onion ring patterns in the SZ at the higher traversing speeds (Fig. 5e–h) were more apparent than those at the lower traversing speeds (Fig. 5a–d). This indicates that increasing the plastic deformation rate of the material is not conducive to alleviating the inhomogeneous structure. At the lower traversing speed of 50 mm/min, the onion ring pattern became more apparent with the rotation rate being further increased to 1200 and 1500 rpm. The result is partially in agreement with that reported by Oh-ishi et al. [30]. Within their studied FSP parameters, as the rotation rate and traversing speed increased, the onion ring structures became distinct in the middle regions of the SZ. This indicates that the increased heat input and enhanced plastic deformation could not eliminate the inhomogeneous microstructure, too.

The onion rings had two types of microstructures. The first type appeared at lower rotation rates, in which the ringlike band was composed of layers of elongated α grains and equiaxed α grains, as well as fine β phase transformation products (Fig. 6a). The second type appeared at higher rotation rates, in which the ring band consisted of layers of Widmanstätten α and layers of mixed equiaxed

α and β transformation products (Fig. 6b). This should be associated with the change of the heat input and material flow resulting from the variation of the rotation rates. At higher rotation rates, the temperature/temperature gradient and strain/strain gradient were higher compared to those at the lower rotation rates. This might result in the generation of the complex microstructure and material flow pattern. This needs more in-depth investigations.

The microstructure appeared in the SZ was parameter dependent and the reason should be mainly attributed to the following factors. First, the processing parameters affected the temperature distribution, and this affected the phase transformation during FSP. Second, the FSP parameters affected the material flow on the passage of the rotation tool, which reflects the displacement fields involving vertical and horizontal components [34]. Cui et al. [35] studied the formation of the “onion ring structure” and analyzed the flow fields around the rotation tool. They considered that the material flow under the shoulder was along horizontal direction caused by the shoulder, so horizontal layer structure was formed in the upper part of the SZ. In the center, the upward and downward flows were closely balanced, and the effects of the horizontal flow pushed by the shoulder could not touch this area, so the onion rings were formed. In fact, the material characteristics can also affect the microstructure in the SZ, such as the grain size [36] and second phase particle-rich bands [37]. The κ phases and β' phase in the BM could affect the material flow pattern, and this is complex and needs further research efforts.

The two pass FSP alleviated the onion ring pattern greatly and increased the area of equiaxed structure in the center of the SZ (Fig. 7), but the banded structure still existed. This means that multiple-pass FSP contributed to homogenizing the SZ microstructure. Thus, more uniform structure was produced in the SZ.

4.2. Formation of banded structure

Although the predominant refinement effect is the dynamic recrystallization due to severe deformation resulting from the FSP, the material self-characteristics should be considered for explaining the inhomogeneous structure of the onion ring in the SZ. As a multiple-phase alloy, the intermetallic κ phases as well as retained β' martensite phase might affect the microstructure evolution of the FSP NAB. For the banded structure appeared in region B, substructure and annealing twins were apparently visible within the α grains, indicating that the recovery and recrystallization occurred simultaneously with phase transformations during FSP. However, from the size and morphology of the α phase it seems that the recrystallization was not complete, i.e., part of the α phase just underwent severe deformation but did not recrystallize. Oh-ishi et al. [31] reported that many low-angle boundaries were observed in the upper region of the SZ, and this implied that part of the α phase was retained without dynamic recrystallization during FSP.

The complete dynamic recrystallization was generally observed in the SZs of friction stir welded (FSW) single phase and quasi-single phase metallic materials, producing fine and uniform equiaxed grains [38–40]. However, this might not be the case for dual or multiple-phase metallic materials. The existence of multiple-phases in the materials would complicate the plastic flow and recrystallization process during FSP. Recently, Xie et al. [41] reported that the incomplete dynamic recrystallization was observed in the SZ of 5 mm thick FSW dual-phase brass (Cu–38Zn alloy) plates. The top and the AS of the SZ were characterized by fine completely recrystallized grains, whereas the remaining region consisted of coarse non-recrystallized deformed grains, annealed recrystallized grains, and deformed recrystallized grains. The occurrence of incomplete recrystallization was attributed to the inhibiting effect of a great amount of remnant fine β' phase (CuZn) which has poor deformation ability and high hardness. Increasing the FSW passes and the tool rotation rates reduced the fraction of non-recrystallized deformed grains, but could not eliminate the incompletely recrystallized zone completely. Considering the existence of intermetallic κ phases and β transformation products in the NAB, it is not surprising that incomplete recrystallization was observed in the FSP NAB.

4.3. Microhardness

The horizontal hardness profiles through the center of the SZ indicated that FSP improved the hardness of the as-cast NAB by about 20% (Fig. 9a). This is mainly attributed to two factors. First, the coarse microstructure of the BM was greatly refined, thereby providing higher hardness according to the Hall–Patch relationship. Second, during FSP, the casting porosities in the BM were closed, which was beneficial to the increase of hardness too. The hardness values as shown in Fig. 9a are similar to the previous reports, in which the hardness values of about 190–220 (Hv) and 190–215 (Hv) were recorded for 9 and 20 mm thick FSP NAB, respectively [24].

The vertical hardness profiles through the center of the SZ revealed that the top and the bottom of the SZ had higher hardness values than the center for both the one pass and the two pass FSP samples (Fig. 9b). This phenomenon is resulted from the inhomogeneous microstructure in the SZ. As discussed above, the microstructure in the SZ can be mainly divided into four parts: Widmanstätten α structure in the surface layer of the SZ, mixture of banded α and β' further below the surface, equiaxed α and martensite β' in the center, and streamlike deformed and dynamic recrystallized structure at the bottom. Mahoney et al. [25] reported that the Widmanstätten α structure in the SZ showed better tensile strength than the equiaxed and lamellar structure, and this may explain why the surface layer exhibited higher hardness values than the central region of the SZ. The bottom region of the SZ was composed of a streamlike fine-grained structure, so it showed higher hardness value than the equiaxed grains in the center. Thus, the hardness values in the top and the bottom of the SZ were higher than those in the center.

It is noted that the two pass FSP did not increase the hardness of the NAB apparently, however, the hardness distribution in the SZ of the two pass FSP became more uniform (Fig. 9a). This was ascribed to more homogeneous microstructure as discussed above. The hardness values in the center of the two pass FSP SZ were similar to those in the one pass FSP SZ for the vertical hardness profiles, and this is in good agreement with the results of the horizontal hardness profiles (Fig. 9b).

4.4. Tensile properties

All the FSP samples exhibited significantly improved tensile strength and ductility compared to the BM (Table 3). The ten-

sile strengths were better than those reported by Palko et al. [24] in which the YS and UTS were 400–420 MPa and 689–724 MPa, respectively, and that reported by Mahoney et al. [25] in which the YS and UTS are 433 MPa and 741 MPa, respectively. Because the mini-tensile specimens were used in this study, it is impossible to compare the present elongation values with the previous ones (14–16% and 23% in Refs. [24,25], respectively). The improvement in the tensile properties of the FSP NAB is ascribed to the elimination of the cast porosities and the refinement of the coarse microstructure, as discussed above.

The tensile properties were apparently parameter dependent. For a constant traversing speed, the YS and UTS of the FSP samples increased firstly and then decreased with increasing the rotation rates. This means that too low or excessive high rotation rates are not beneficial to the increase of the tensile strength. For a constant rotation rate of 1500 rpm, the UTS increased firstly and then decreased with increasing the traversing speed. This indicates that medium traversing speeds produced better strengthening effect on the NAB alloy. The results might be associated with the variation of heat input and material plastic deformation. At lower rotation rates or higher traverse speeds, the heat input was lower and was not enough to ensure full plastic deformation. However, at higher rotation rates or lower traverse speeds, the heat input was higher and resulted in the dissolution of many κ particles, decreasing the strength of the FSP samples.

For the one pass FSP samples, the FSP-800/50 samples showed the lowest elongation, whereas the FSP-1000/50, FSP-1200/50, and FSP-1500/50 samples exhibited better ductility than the others. The results should be attributed to the microstructure evolution in the SZ. As mentioned above, the SZ of the FSP-800/50 sample showed apparently inhomogeneous microstructure in the SZ, and this inhomogeneous structure is not conducive to the ductility; the FSP-1000/50, FSP-1200/50, and FSP-1500/50 samples exhibited more homogeneous microstructure in the SZ with larger area of equiaxed grain structure, so they showed better ductility. The two pass FSP did not affect the tensile strength of the FSP samples apparently, but it improved the elongation of the samples considerably. Because the one pass FSP has effectively eliminated the porosities and refined the microstructure in the as-cast NAB, the two pass FSP would improve little on this respect. This resulted in less increase in the tensile strength. However, the two pass FSP further homogenized the microstructures and produced larger area of equiaxed grain structure, and this resulted in the increase in the elongation.

5. Conclusions

1. The microstructure of the as-cast NAB was greatly refined and densified by FSP. The SZ was characterized by inhomogeneous microstructure, and the inhomogeneous microstructure was parameters dependent.
2. The SZs for all FSP parameters could be divided into four sub-regions from the surface to the bottom: fine Widmanstätten primary α phase in the surface layer, banded primary α and β' phases in the subsurface layer, equiaxed α and β' phases with a size of less than 10 μm in the center, and streamlike α and β' phases at the bottom.
3. The banded α structure appeared in the subsurface layer of the SZ resulted from the incomplete dynamic recrystallization and intense plastic deformation of FSP.
4. The average hardness value of the FSP NAB was about 20% higher than that of the BM. The center of the SZ showed slightly lower hardness values compared to the top and the bottom.
5. The tensile properties of the one-pass FSP NAB were greatly improved compared to those of the BM. The YS, UTS, and elongation of the FSP samples were 436–502 MPa, 790–852 MPa,

and 20–29%, respectively, along the transverse direction, and 415–479 MPa, 776–837 MPa, and 25–31%, respectively, along the longitudinal direction.

6. The tensile properties were parameter dependent. The rotation rate in the range of 1000–1500 rpm and the traversing speed in the range of 50–100 mm/min produced better tensile properties.
7. The two pass FSP produced more homogeneous structure in the SZ, but it could not eliminate the inhomogeneous structure completely.
8. The two pass FSP did not increase the tensile strength of the one pass FSP NAB, but increased the ductility by 28%. Furthermore, two pass FSP improved the hardness distribution uniformity in the SZ without noticeable variation in the average hardness value.

Acknowledgements

This work was supported by the National Outstanding Young Scientist Foundation under Grant No. 50525103, the National Basic Research Program of China under Grant No. 2006CB605205, the National High-tech Research Program under Grant No. 2006AA03Z111, and the Hundred Talents Program of Chinese Academy of Sciences.

References

- [1] W.M. Thomas, E.D. Nicholas, J.C. Needham, M.G. Murch, P. Templesmith, C.J. Dawes, G.B., Patent Application No. 9125978.8 (December 1991).
- [2] C.J. Dawes, W.M. Thomas, *Weld. J.* 75 (1996) 41–45.
- [3] W.M. Thomas, R.E. Dolby, Materials, ASM Int., Park, OH, USA, 2003, pp. 203–211.
- [4] R.S. Mishra, Z.Y. Ma, *Mater. Sci. Eng. R* 50 (2005) 1–78.
- [5] R.S. Mishra, M.W. Mahoney, S.X. McFadden, N.A. Mara, A.K. Mukherjee, *Scripta Mater.* 42 (2000) 163–168.
- [6] R.S. Mishra, M.W. Mahoney, ICSAM-2000, 357-3, 2001, pp. 507–512.
- [7] P.B. Berbon, W.H. Bingel, R.S. Mishra, C.C. Bampton, M.W. Mahoney, *Scripta Mater.* 44 (2001) 61–66.
- [8] R.S. Mishra, Z.Y. Ma, I. Charit, *Mater. Sci. Eng. A* 341 (2002) 307–310.
- [9] A.S. Zarghani, S.F.K. Bozorg, A.Z. Hanzaki, *Mater. Sci. Eng. A* 500 (2009) 84–91.
- [10] C.J. Hsu, C.Y. Chang, P.W. Kao, N.J. Ho, C.P. Chang, *Acta Mater.* 54 (2006) 5241–5249.
- [11] C.H. Chuang, J.C. Huang, P.J. Hsieh, *Scripta Mater.* 53 (2005) 1455–1460.
- [12] Z.Y. Ma, S.R. Sharma, R.S. Mishra, *Metall. Mater. Trans. A* 37A (2006) 3323–3336.
- [13] E.A. Culpan, G. Rose, *Br. Corros. J.* 14 (1979) 160–166.
- [14] R.J. Ferrara, T.E. Caton, *Mater. Perform.* 2 (1982) 30–34.
- [15] G.W. Lorimer, F. Hasan, J. Iqbal, N. Ridley, *Br. Corros. J.* 21 (1986) 244–248.
- [16] A. Al-Hashem, W. Riad, *Mater. Charact.* 48 (2002) 37–41.
- [17] C.H. Tang, F.T. Cheng, H.C. Man, *Mater. Sci. Eng. A* 373 (2004) 195–203.
- [18] E.A. Culpan, G. Rose, *J. Mater. Sci.* 13 (1978) 1647–1657.
- [19] M. Sahoo, *Trans. AFS* 90 (1982) 913–926.
- [20] A. Jahanafrooz, F. Hasan, G.W. Lorimer, N. Ridley, *Metall. Trans. A* 14A (1983) 1951–1956.
- [21] E.A. Feest, I.A. Cook, *Met. Technol.* 10 (1983) 121–124.
- [22] F. Hasan, J. Iqbal, N. Ridley, *Mater. Sci. Technol.* 1 (1985) 312–315.
- [23] F. Hasan, A. Jahanafrooz, G.W. Lorimer, N. Ridley, *Metall. Trans. A* 13A (1982) 1337–1345.
- [24] W.A. Palko, R.S. Fielder, P.F. Young, *Mater. Sci. Forum* 426–432 (2003) 2909–2914.
- [25] M.W. Mahoney, W.H. Bingel, S.R. Sharma, R.S. Mishra, *Mater. Sci. Forum* 426–432 (2003) 2843–2848.
- [26] C.B. Fuller, M.W. Mahoney, W.H. Bingel, M. Calabrese, B. London, *Mater. Sci. Forum* 539–543 (2007) 3751–3756.
- [27] P.S. Prevey, D.J. Hornbach, D.N. Jayaraman, *Mater. Sci. Forum* 539–543 (2007) 3807–3813.
- [28] K. Oh-ishi, T.R. McNelley, *Metall. Mater. Trans. A* 35A (2004) 2951–2961.
- [29] K. Oh-ishi, A.M. Cuevas, D.L. Swisher, T.R. McNelley, *Mater. Sci. Forum* 426–432 (2003) 2885–2890.
- [30] K. Oh-ishi, T.R. McNelley, *Metall. Mater. Trans. A* 36A (2005) 1575–1585.
- [31] K. Oh-ishi, A.P. Zhilyaev, T.R. McNelley, *Metall. Mater. Trans. A* 37A (2006) 2239–2251.
- [32] T.R. McNelley, K. Oh-ishi, A.P. Zhilyaev, *Mater. Sci. Forum* 539–543 (2007) 3745–3750.
- [33] M.D. Fuller, S. Swaminathan, A.P. Zhilyaev, T.R. McNelley, *Mater. Sci. Eng. A* 463 (2007) 128–137.
- [34] T.U. Seidel, A.P. Reynolds, *Metall. Mater. Trans. A* 32A (2001) 2879–2884.
- [35] G.R. Cui, Z.Y. Ma, S.X. Li, *Scripta Mater.* 58 (2008) 1082–1085.
- [36] H. Jin, S. Saimoto, M. Ball, P.L. Threadgill, *Mater. Sci. Technol.* 17 (2001) 1605–1614.
- [37] M.A. Sutton, B. Yang, A.P. Reynolds, R. Taylor, *Mater. Sci. Eng. A* 323 (2002) 160–166.
- [38] G.M. Xie, Z.Y. Ma, L. Geng, *Scripta Mater.* 57 (2007) 73–76.
- [39] K.V. Jata, S.L. Semiatin, *Scripta Mater.* 43 (2000) 743–749.
- [40] G.M. Xie, Z.Y. Ma, L. Geng, R.S. Chen, *Mater. Sci. Eng. A* 471 (2007) 63–68.
- [41] G.M. Xie, Z.Y. Ma, L. Geng, *Philos. Mag.* 89 (2009) 1505–1516.